Supporting Information

TABLE OF CONTENTS

Table S1. Crystallographic data and refinement for **1Er–7Y**

formula	$C_{13}H_{14}BEr$	$C_{14}H_{16}BEr$	$C_{17}H_{23}BNEr$	$C_{13}H_{14}BDy$	$C_{14}H_{16}BDy$	$C_{17}H_{23}BNDy$	$C_{17}H_{23}BNY$
fw	348.31	362.34	419.43	343.55	357.58	414.67	341.08
cryst syst	$P2_1/c$	$P2_1/c$	$P2_1/c$	$P2_1/c$	$P2_1/c$	$P2_1/c$	$P2_1/c$
space group	monoclinic	monoclinic	monoclinic	monoclinic	monoclinic	monoclinic	monoclinic
a, Å	11.392(2)	12.4425(17)	17.008(4)	11.484(7)	12.4412(12)	16.956(3)	16.957(6)
b, Å	8.2764(16)	8.8385(12)	8.486(2)	8.335(5)	8.8630(8)	8.5607(13)	8.521(3)
c, Å	12.051(2)	11.5467(16)	11.489(3)	12.088(8)	11.6155(11)	11.4844(18)	11.457(4)
V, $Å^3$	1115.7(4)	1256.8(3)	1626.4(7)	1136.9(12)	1268.4(2)	1635.3(4)	1623.9(9)
Z	4	4	4	4	4	4	4
T , K	140(2)	133(2)	133(2)	140(2)	143(2)	133(2)	140(2)
F(000)	660	692	820	652	684	812	704
D_C, g cm^{-3}	2.074	1.915	1.713	2.007	1.873	1.684	1.395
μ, mm^{-1}	7.481	6.644	5.149	6.532	5.859	4.558	3.581
λ, Å	0.71073	0.71073	0.71073	0.71073	0.71073	0.71073	0.71073
Cryst size, mm^3	0.24×0.16×0.01	0.25×0.20×0.15	0.35×0.25×0.12	0.20×0.15×0.01	0.35×0.28×0.22	0.30×0.20×0.04	0.26×0.22×0.02
T min, T max	0.2669, 0.9289	0.2874, 0.4356	0.2659, 0.5770	0.3550, 0.9376	0.2336, 0.3589	0.3417, 0.8387	0.4562, 0.9318
θ min, θ max, deg	1.82, 30.79	2.84, 30.14	2.69, 30.06	3.04, 23.88	2.83, 30.55	2.45, 30.53	2.45, 26.27
R1 [$I \geq 2\sigma(I)$]	0.0528	0.0231	0.0433	0.0724	0.0157	0.0465	0.0589
wR2 (all data)	0.1596	0.0497	0.1490	0.2269	0.0393	0.1220	0.1495
S	1.038	1.051	1.023	1.010	1.110	1.022	0.990
max and mean Δ /σ	0.000, 0.000	0.001, 0.000	0.001, 0.000	0.031, 0.003	0.007, 0.000	0.001, 0.000	0.005, 0.001

Table S2. Selected Distances (Å) and Dihedral Angles (deg) for **1Er**–**6Dy**						
Complex	**1Er**	**2Er**	**3Er**	**4Dy**	**5Dy**	**6Dy**
Ln–C(COT)[a]	2.495(8)	2.491(2)	2.493(5)	2.519(3)	2.514(2)	2.518(7)
Ln–C(BZ)[a]	2.661(8)	2.657(3)	2.647(4)	2.697(3)	2.688(3)	2.679(7)
Ln–B	2.76(1)	2.779(3)	2.83(1)	2.79(2)	2.818(2)	2.86(1)
Ln–Centroid of COT	1.676	1.674	1.679	1.711	1.711	1.718
Ln–Centroid of BZ	2.257	2.245	2.254	2.307	2.285	2.277
Dihedral angle	10.6(2)	5.5(1)	9.3(1)	11.8(5)	6.4(1)	10.9(1)
B–Plane of BZ	0.028	0.059	0.098	0.059	0.059	0.109
BZ represents boratabenzene ring. [a] Average value.						

Table S3: Kramers doublets (KDs) energy spectrum (cm^{-1}), *g*-tensor of ground and excited KDs for **1Er**–**3Er**

KDs	**1Er**			**2Er**			**3Er**		
	E			*E*			*E*		
1	0.0			0.0			0.0		
2	148.7			174.0			158.8		
3	201.0			223.5			194.3		
4	213.0			227.7			227.8		
5	240.5			244.3			248.8		
6	250.6			254.3			258.2		
7	271.4			263.9			273.9		
8	295.6			279.9			300.1		
KDs	g_x	g_y	g_z	g_x	g_y	g_z	g_x	g_y	g_z
1	0.00015	0.0002	17.872	0.0001	0.0001	17.886	0.0025	0.0028	17.808
2	0.015	0.018	16.333	0.020	0.029	15.453	0.318	0.464	15.046
3	0.608	1.340	14.499	0.667	1.528	12.060	0.171	0.991	14.652
4	0.377	2.069	10.881	0.219	3.275	12.269	4.232	5.683	7.190
5	2.716	3.509	7.656	9.499	5.605	1.069	1.321	3.672	7.911
6	1.936	4.443	7.377	0.185	2.461	11.869	0.270	3.680	9.984
7	0.244	1.147	14.571	7.674	5.778	3.095	1.355	2.106	12.579
8	0.099	0.151	16.070	0.160	0.245	14.451	0.174	0.381	15.816

Table S4: Kramers doublets (KDs) energy spectrum (cm^{-1}), *g*-tensor of ground and excited KDs for **4Dy**–**6Dy**

KDs	**4Dy**			**5Dy**			**6Dy**		
	E			*E*			*E*		
1	0.0			0.0			0.0		
2	56.2			33.6			39.7		
3	83.6			51.2			62.9		
4	103.0			82.4			97.4		
5	138.2			106.9			120.4		
6	157.9			121.5			161.7		
7	274.2			263.2			244.4		
8	540.1			503.5			519.9		
KDs	g_x	g_y	g_z	g_x	g_y	g_z	g_x	g_y	g_z
1	0.050	0.090	18.839	0.079	0.337	17.539	0.108	0.148	19.111
2	0.498	0.837	14.665	0.308	0.470	12.925	1.116	2.788	16.035
3	2.674	3.077	15.398	2.710	4.707	13.978	4.504	5.331	7.881
4	8.914	6.071	0.859	1.367	4.864	8.625	7.928	5.572	0.279
5	0.762	4.699	9.079	1.696	6.005	12.839	2.039	3.059	11.851
6	1.185	2.946	13.582	0.527	1.258	13.684	0.215	0.606	18.070
7	0.006	0.008	17.344	0.000	0.000	17.337	0.007	0.012	17.251
8	0.000	0.000	19.880	0.000	0.000	19.893	0.000	0.000	19.877

Figure S1: Molecular structures of **4Dy**–**6Dy**. Color code: orange, Dy; dark grey, C; yellow, B; blue, N. Hydrogen atoms are omitted for clarity.

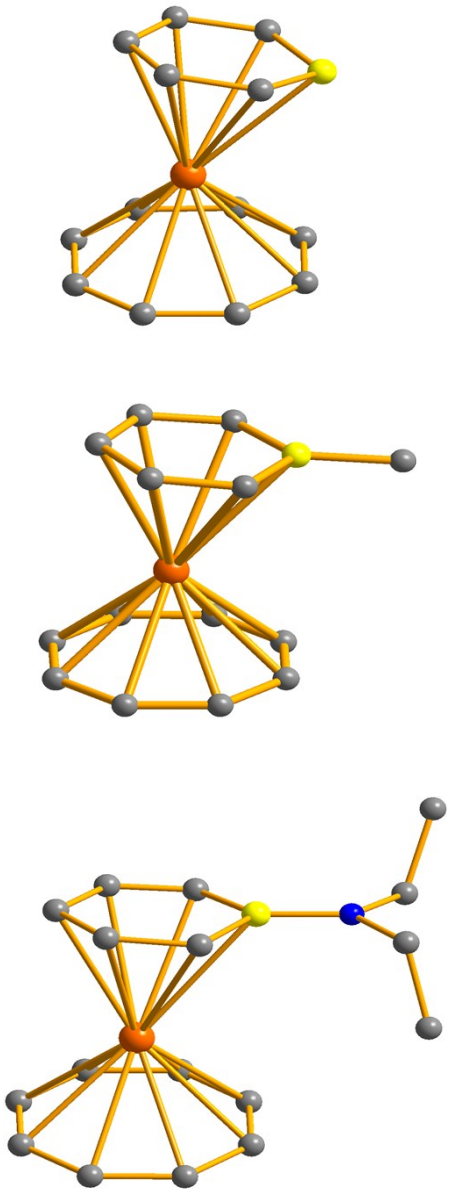

Figure S2: Packing diagrams for **1Er–3Er** ((a)–(c)) shown along the corresponding crystalline axis. Light blue dashes represent the edge to face π···π stacking interaction.

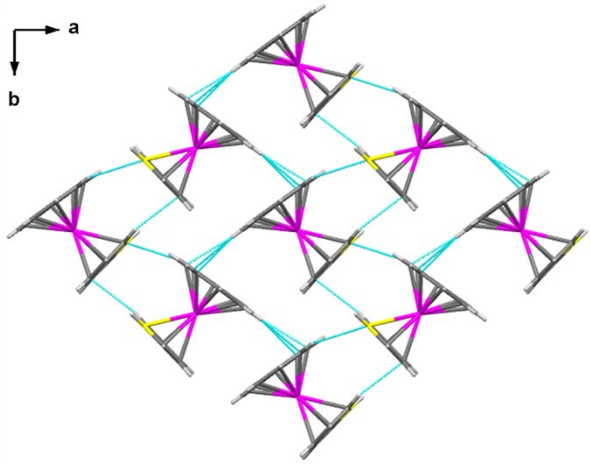

(a)

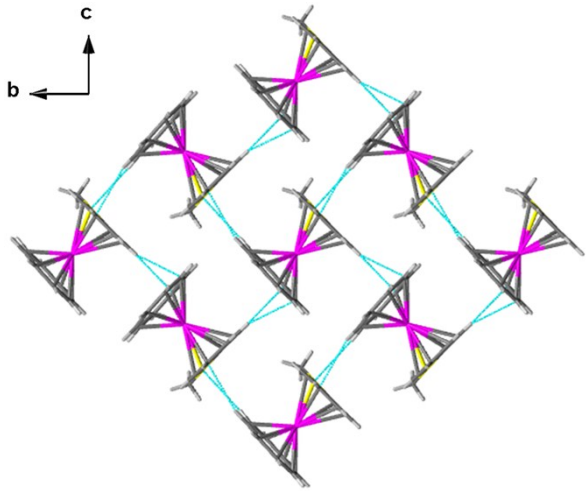

(b)

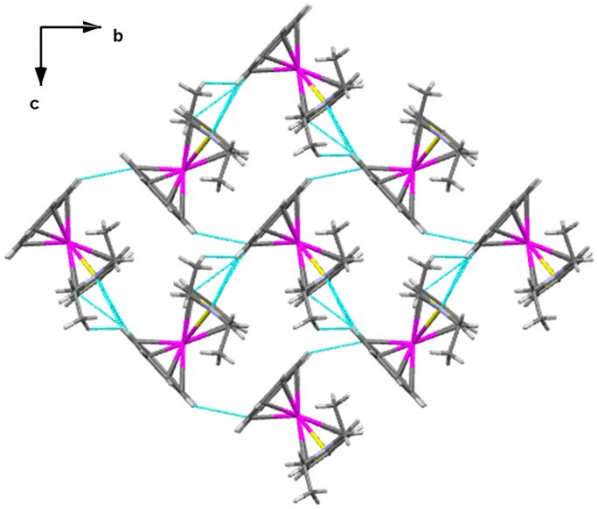

(c)

Figure S3: Packing diagrams for **4Dy–6Dy** shown along the corresponding crystallographic axis. Light blue dashes represent the edge to face π···π stacking interaction.

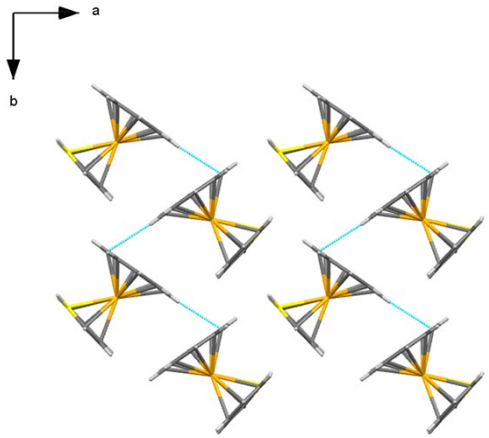

(a)

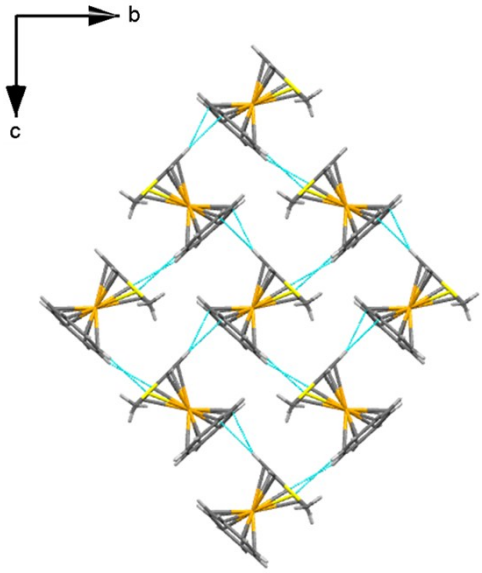

(b)

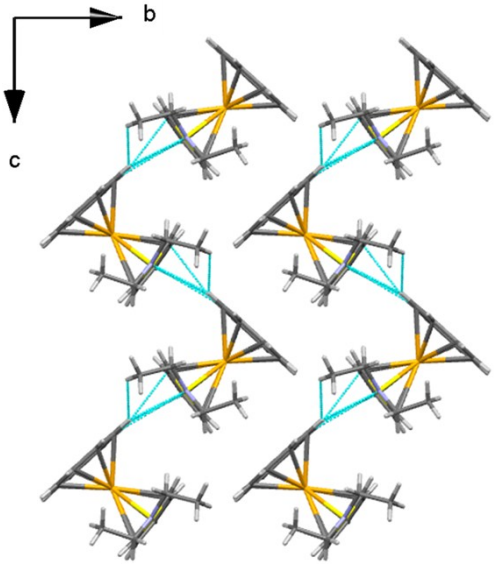

(c)

Figure S4: $\chi_m T$ vs. T plots for **4Dy–6Dy**

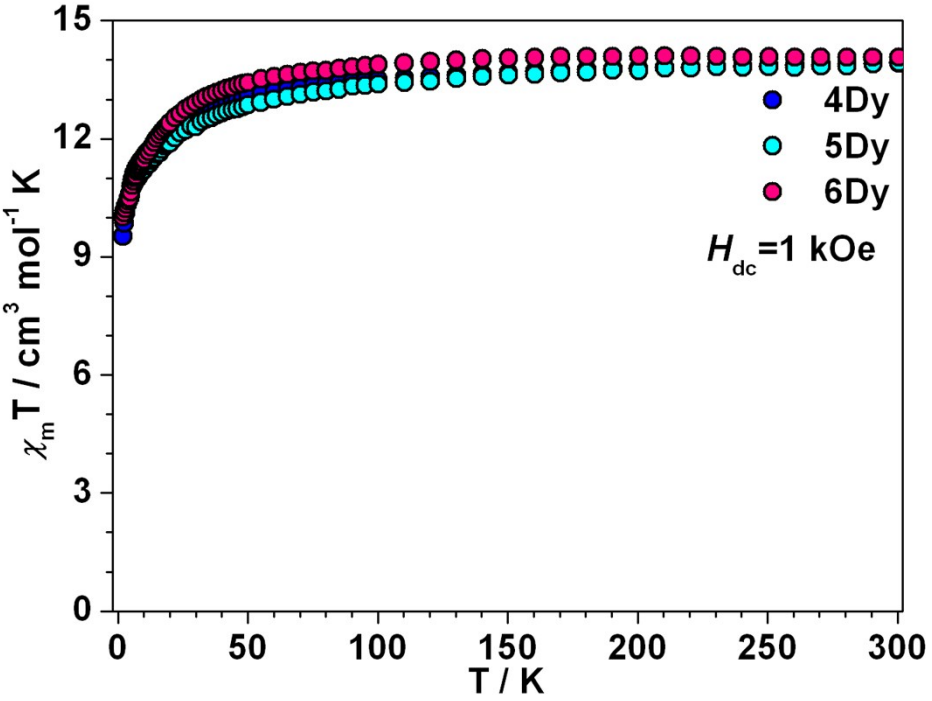

Figure S5: Field cooling $\chi_m T$ vs. T plots under selected dc fields for **1Er**.

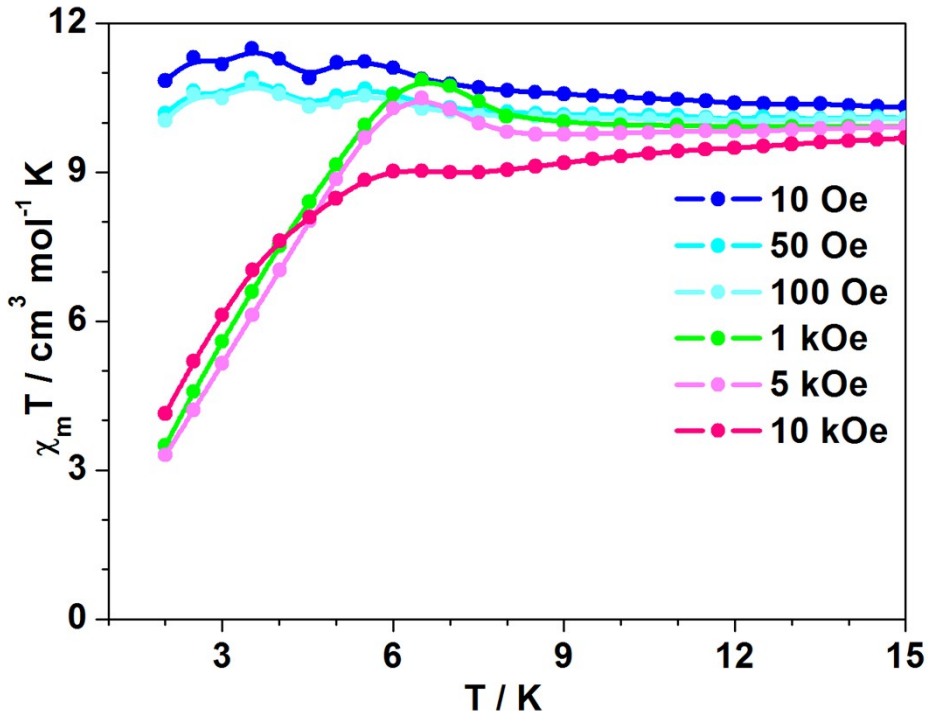

Figure S6: Frequency dependence ac magnetization measurement, χ_m' vs. ν plots under zero dc field for **1Er**(a), **2Er**(b) and **3Er**(c).

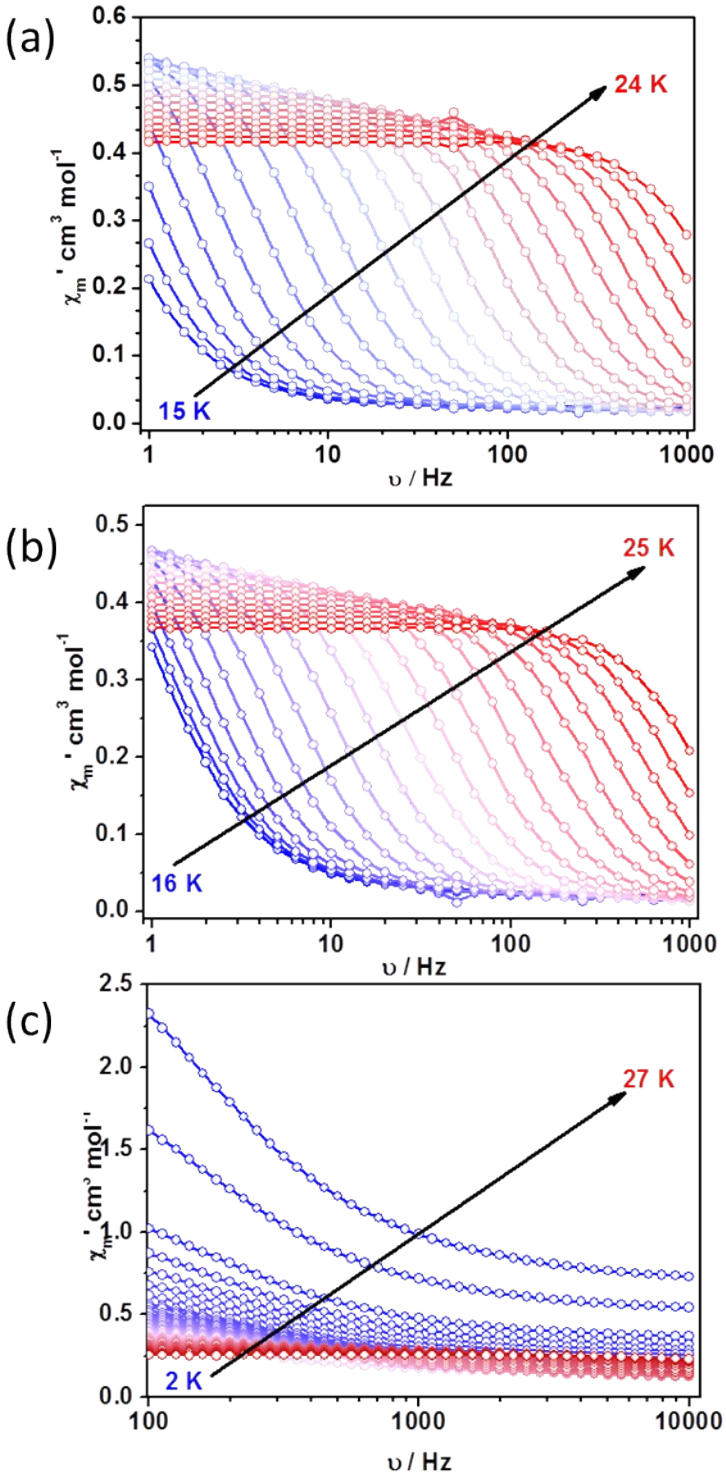

Figure S7: Temperature dependence ac magnetization measurement, χ_m' and χ_m'' vs. *T* plots at different frequencies under zero dc field for **1Er**

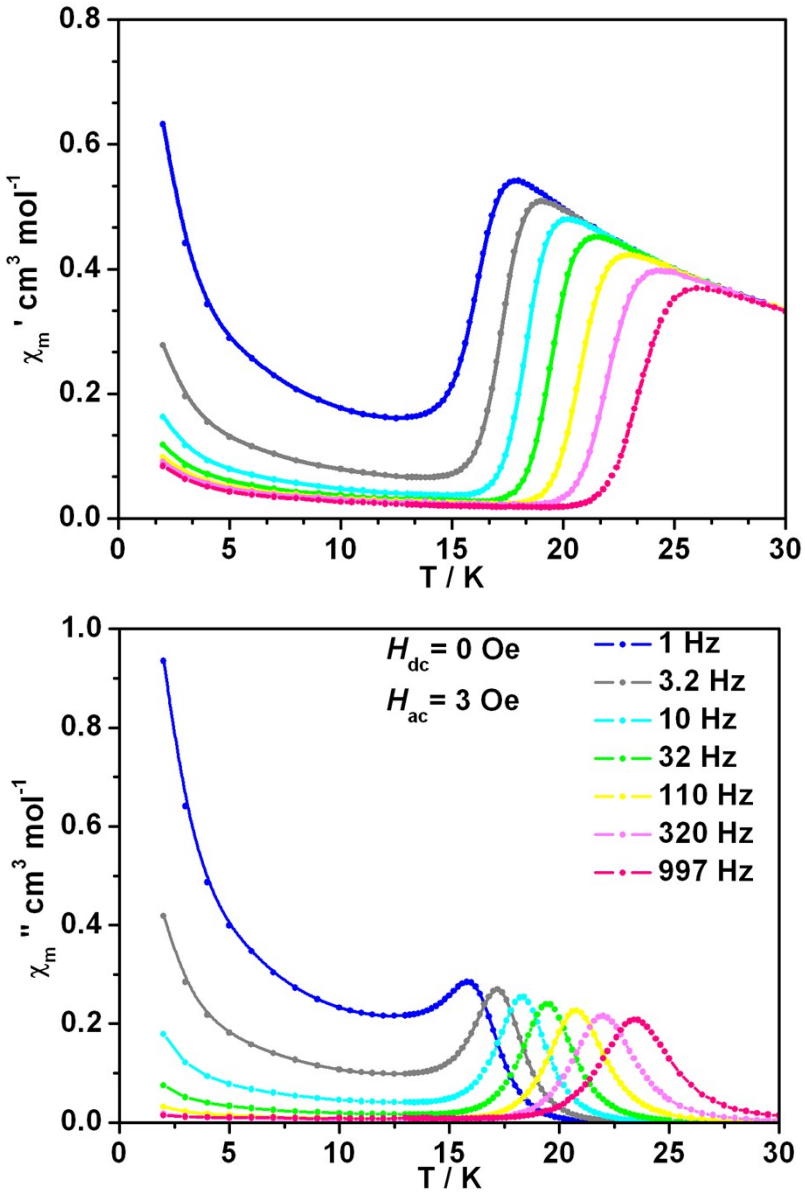

Figure S8: Temperature dependence ac magnetization measurement, χ_m' and χ_m'' vs. *T* plots at different frequencies under zero dc filed for **2Er**

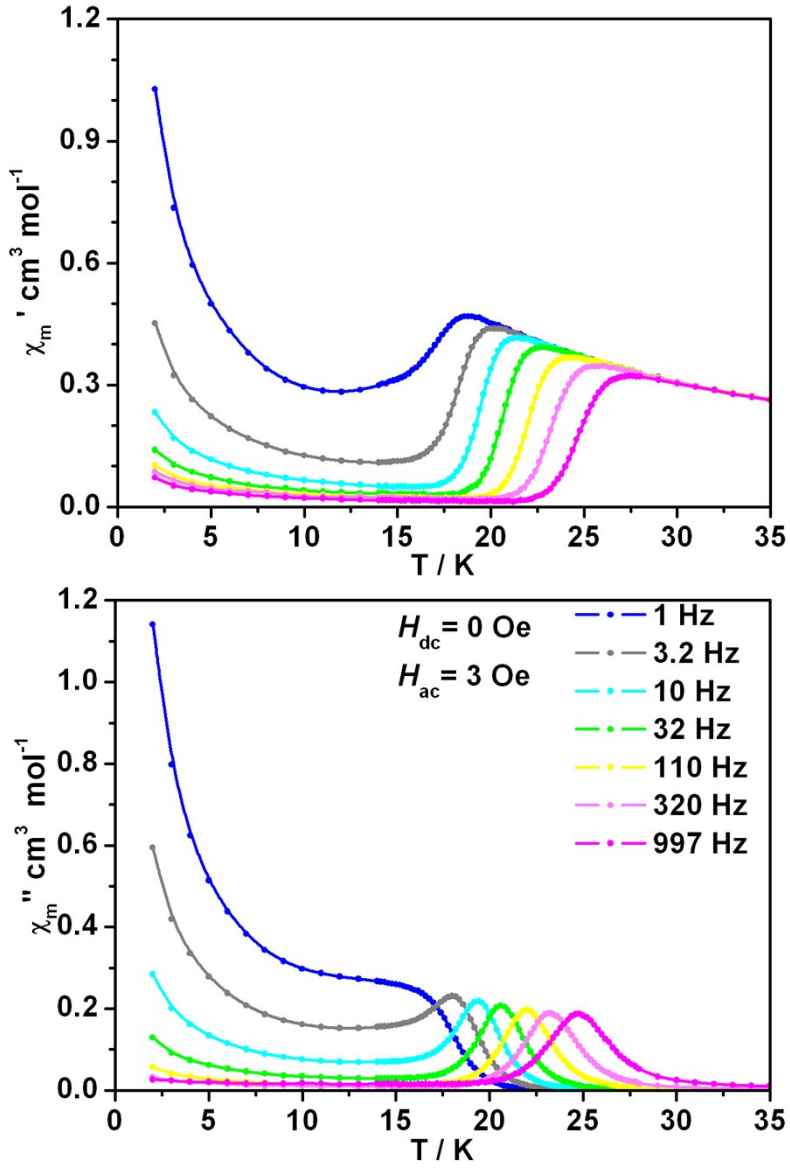

Figure S9: Frequency dependence ac magnetization measurement, χ_m' and χ_m'' vs. ν plots below 10 K under zero dc filed for **1Er** (a) and **2Er** (b)

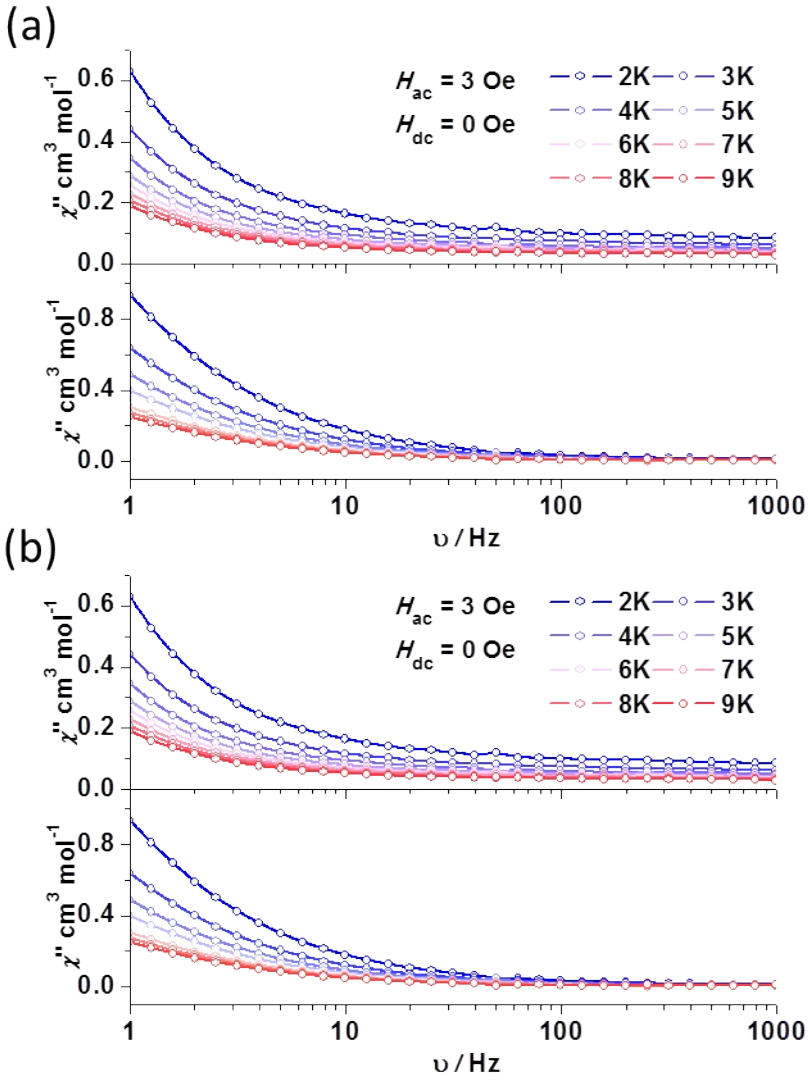

Figure S10: Col-Cole plots for **1Er**(a), **2Er**(b) and **3Er**(c) by using the generalized Debye model. The distribution of relaxation time (α) is small (α: 0.007-0.042 for **1Er**; α: 0.008-0.054 for **2Er**; α: 0.015-0.234 for **3Er**)

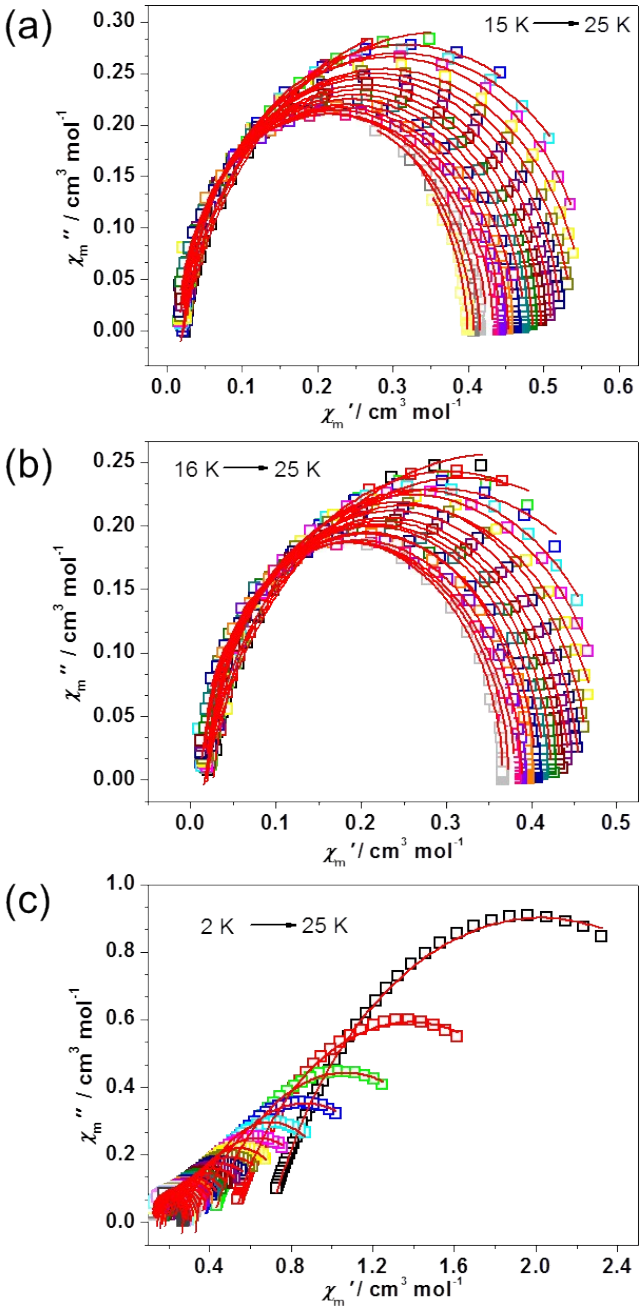

Figure S11: Expend view of χ_m'' vs. ν plots of **3Er**

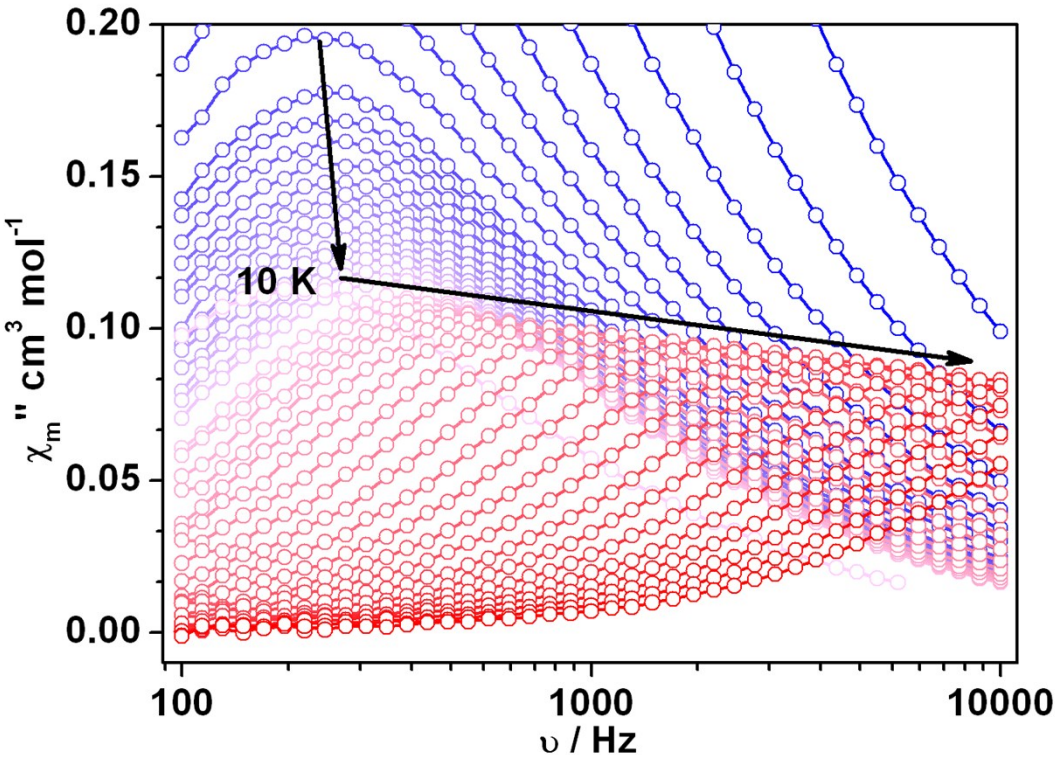

Figure S12: Temperature dependence ac magnetization measurement, χ_m' and χ_m'' vs. *T* plots at different frequencies under 2 kOe dc field for **3Er**

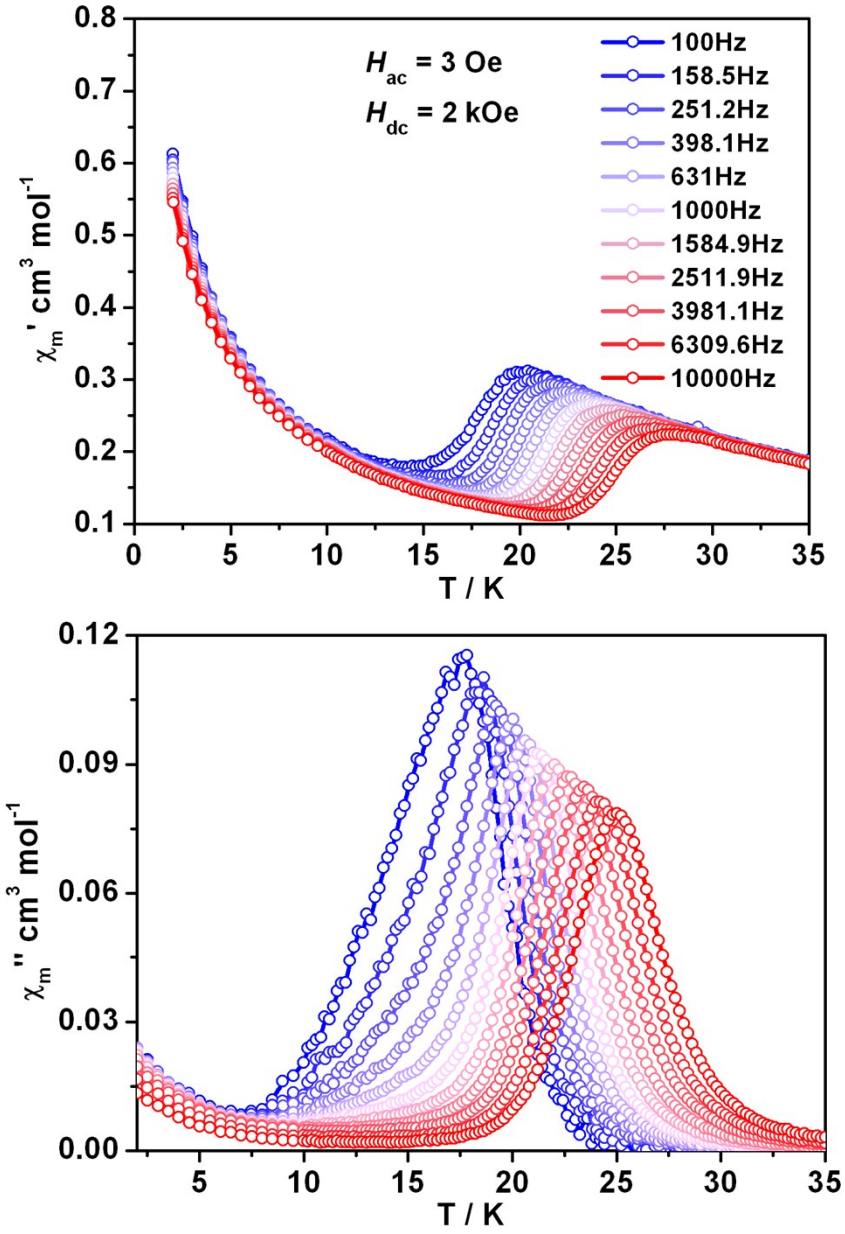

Figure S13: Dynamic ac susceptibility measurement and the relaxation time τ vs. the inverse of temperature T^{-1} diagram for **4Dy**

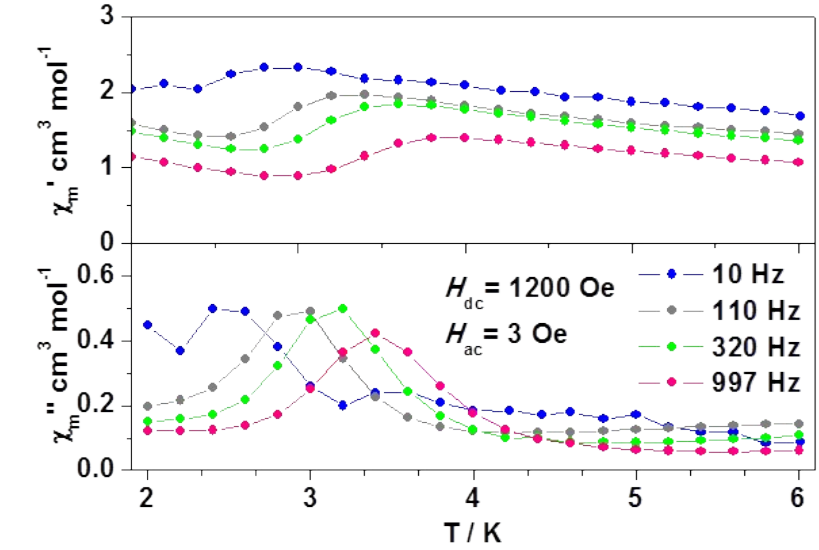

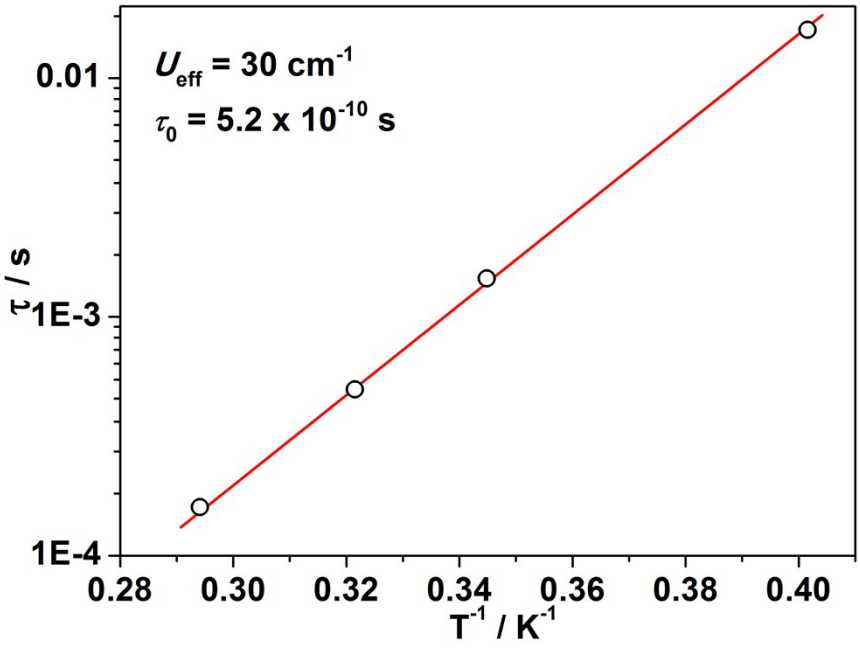

Figure S14: Dynamic ac susceptibility measurement and the relaxation time τ vs. the inverse of temperature T^{-1} diagram for **5Dy**

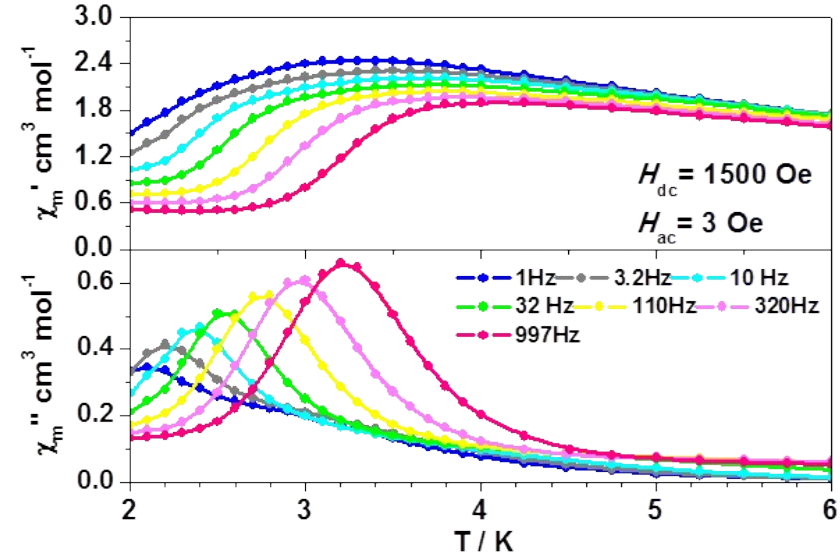

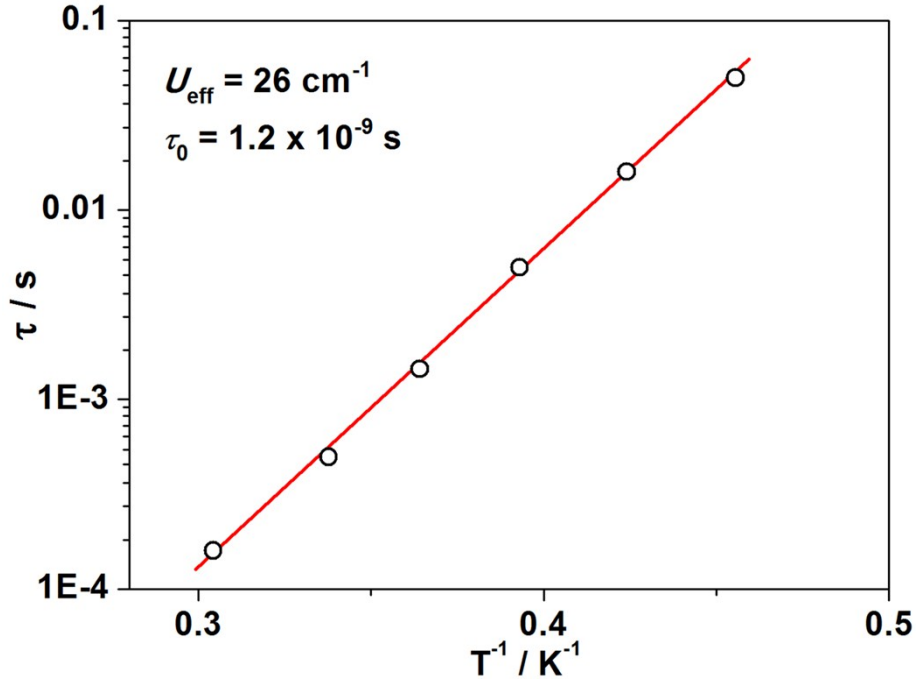

Figure S15: Dynamic ac susceptibility measurement and the relaxation time τ vs. the inverse of temperature T^{-1} diagram for **6Dy**

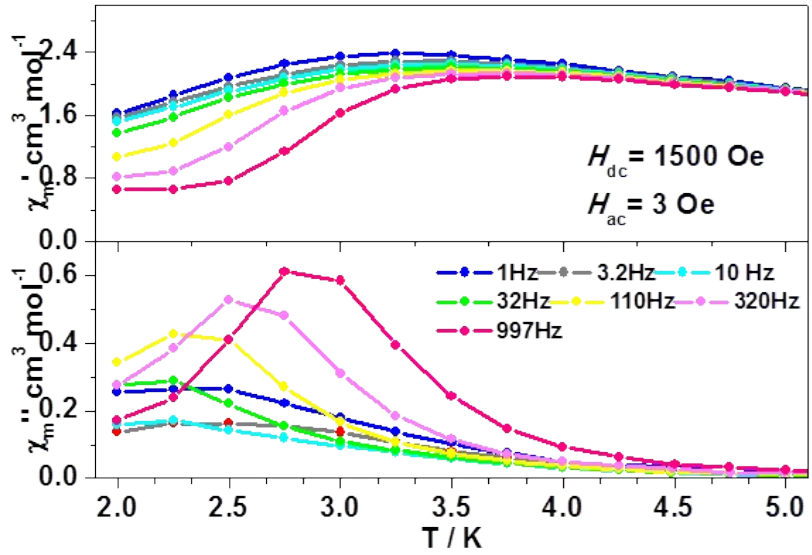

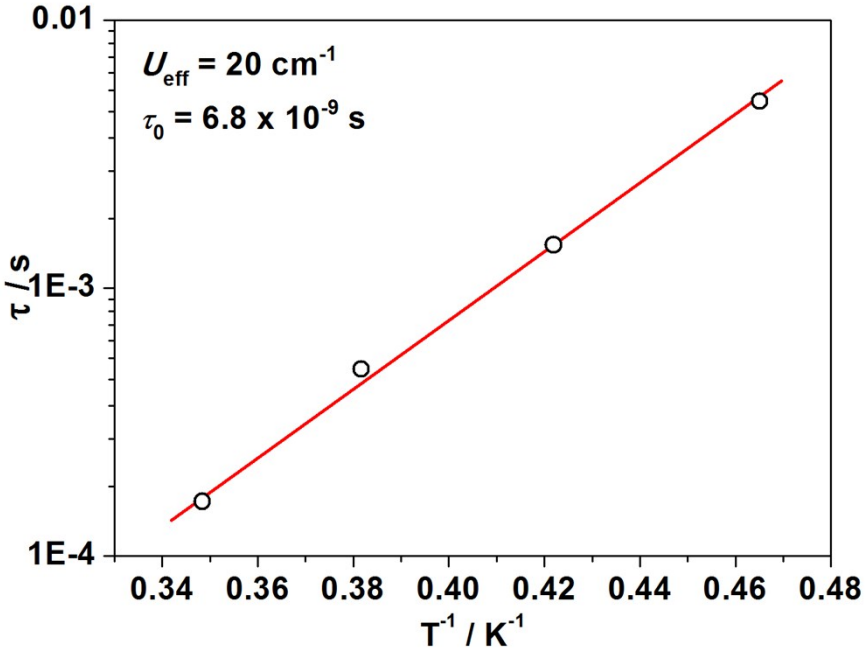

Figure S16: Temperature dependence ac magnetization measurement, χ_m' and χ_m'' vs. *T* plots at different frequencies under zero dc field for diluted **3Er**. The poor signals are properly due to the less magnetic samples.

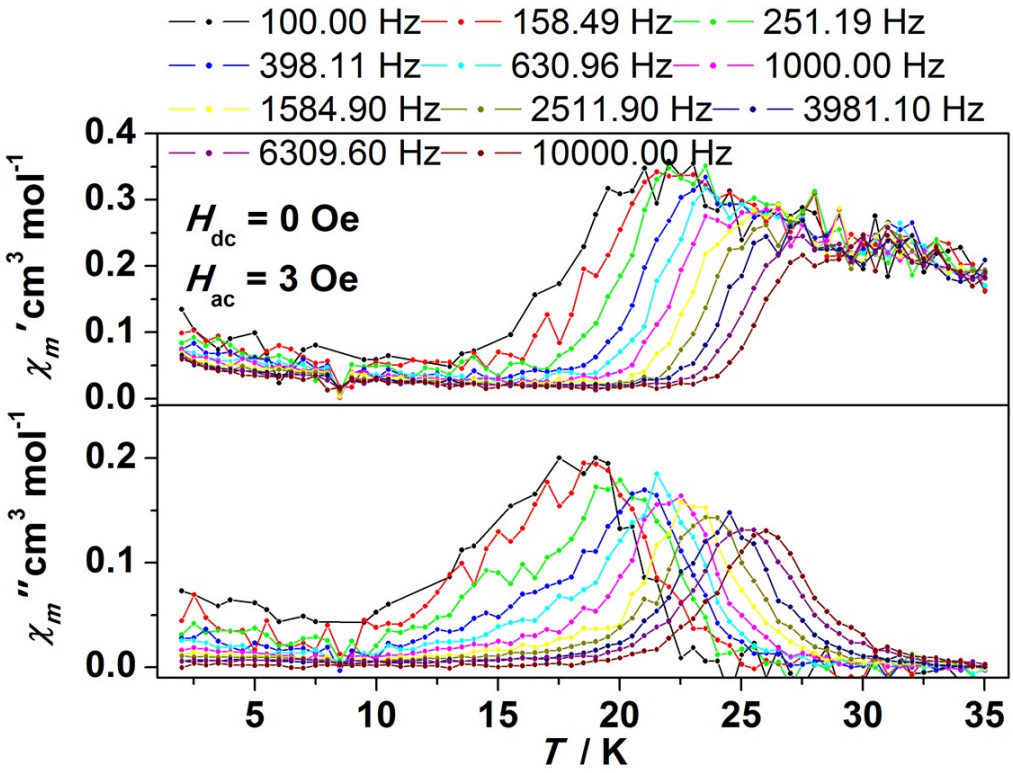

Figure S17: The relaxation time τ vs. the inverse of temperature T^{-1} diagram for diluted **3Er**

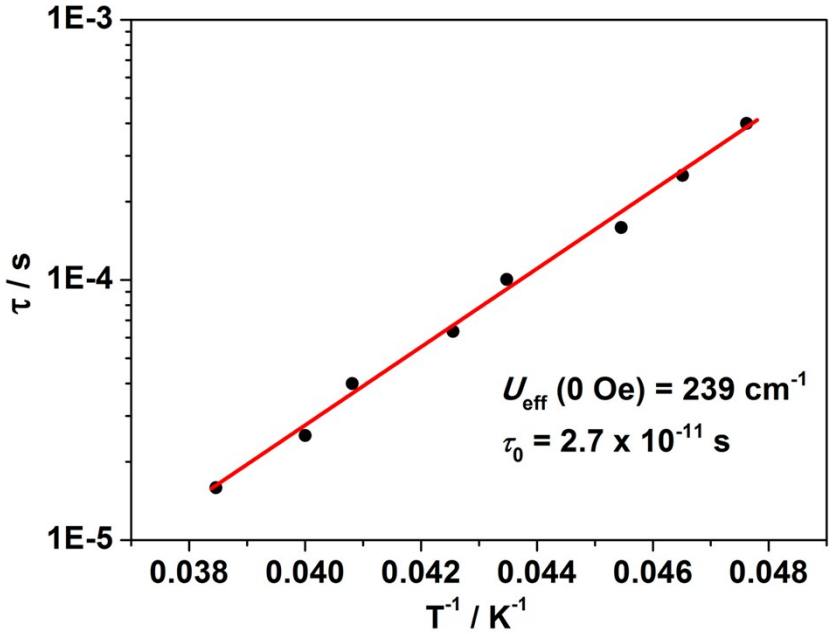

Figure S18: Orientation of the local main magnetic axes of the ground Kramers doublet on Er^{III}complexes **1Er**–**3Er**((a)–(c)) and Dy^{III} complexes **4Dy**–**6Dy**((d)–(f)).

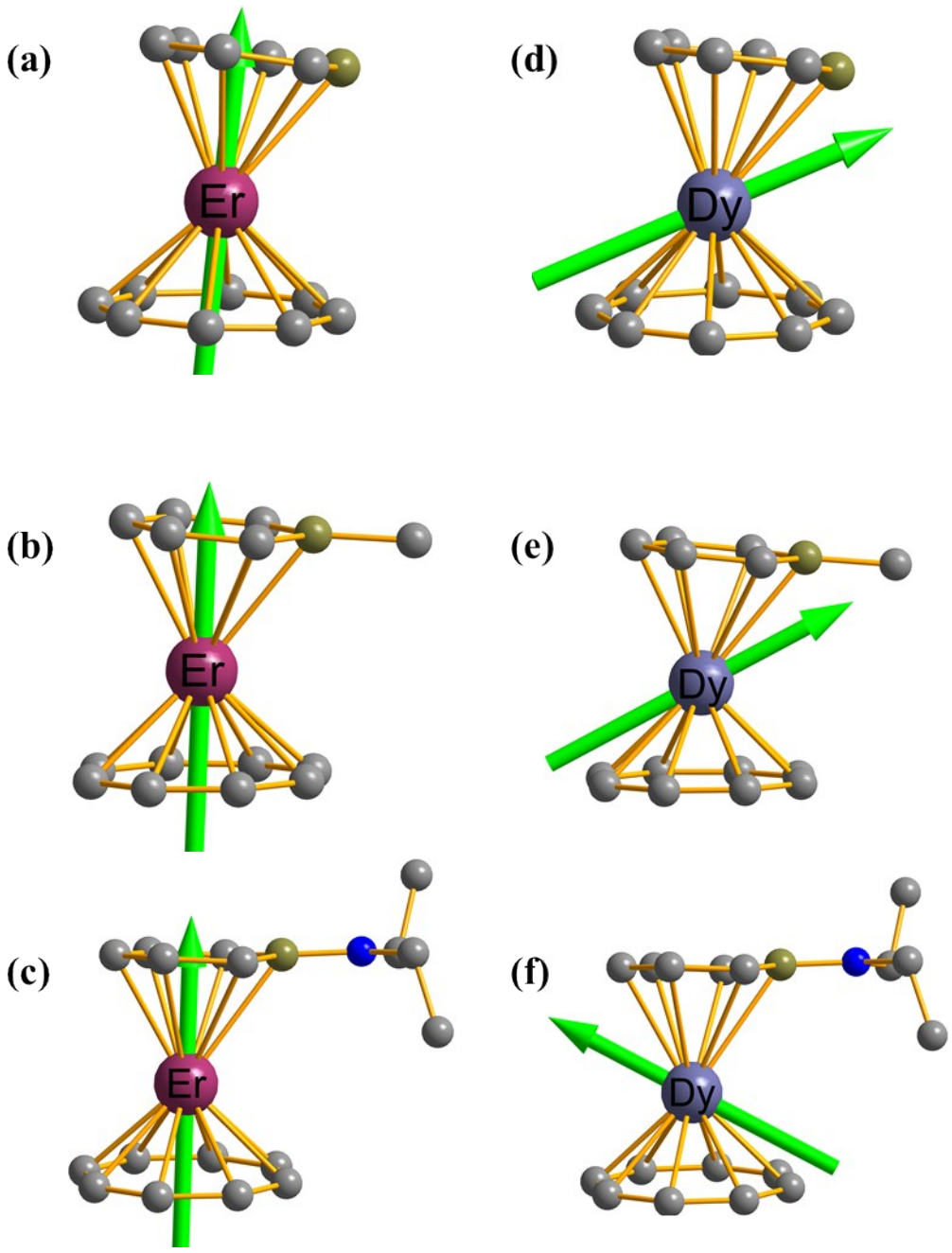

Figure S19: $\chi_m T$ vs. T plots for **1Er** measured among cooling at selected balancing time.

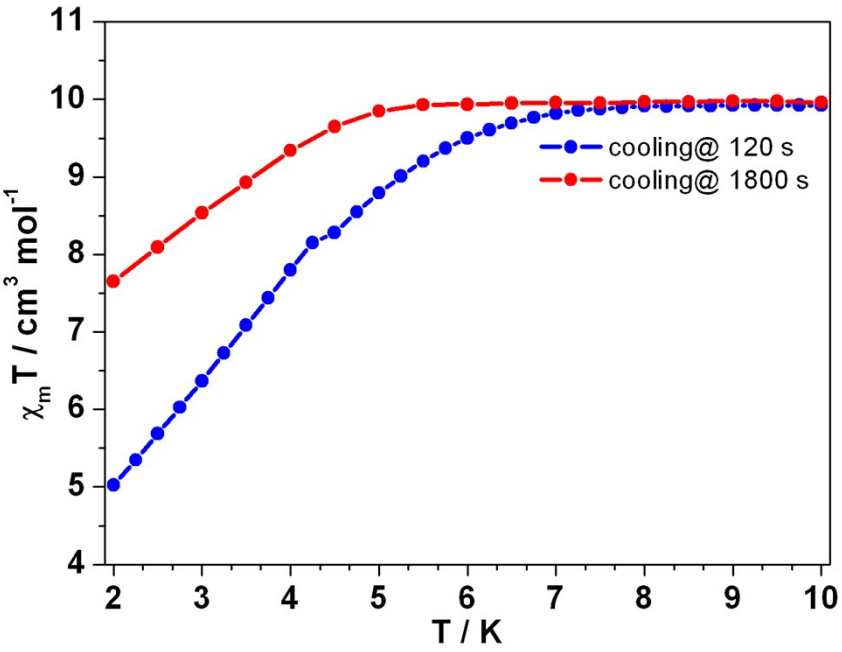

Figure S20: $\chi_m T$ vs. Time plot for **1Er**, the sample was cooled under zero field.